FDTD Analysis of Electromagnetic Wave Radiation from Systems Containing Horn Antennas

Daniel S. Katz, *Student Member, IEEE*, Melinda J. Piket-May, *Student Member, IEEE*, Allen Taflove, *Fellow, IEEE*, and Korada R. Umashankar, *Senior Member, IEEE*

Abstract—**The application of the finite-difference time-domain (FDTD) method to various radiating structures is considered. These structures include two- and three-dimensional waveguides, flared horns, a two-dimensional parabolic reflector, and a two-dimensional hyperthermia application. Numerical results for the horns, waveguides, and parabolic reflectors are compared with results from method of moments (MM). The results for the hyperthermia application are shown as extensions of the previously validated models. This new application of the FDTD method is shown to be useful when other numerical or analytic methods cannot be applied.**

I. Introduction

THIS paper will attempt to validate the finite-difference time domain (FDTD) code when used for the modeling of both two- and three-dimensional radiating structures. It will use waveguides, flared horns, and parabolic reflectors as examples that will be validated against method of moments (MM) codes. There are no published examples of previous use of the FDTD method to solve problems involving a radiating object.

Previously, for work such as this, high-frequency approximations and MM have been used. Most high-frequency methods are based on the geometric theory of diffraction (GTD), which was introduced by Keller [1], [2] in the late 1950's. GTD has also been used recently to study a pyramidal horn, as part of a complex system in which the horn fed an offset reflector [3]. The horn was modeled using GTD, and asymptotic physical optics (APO) was used to model the reflector illuminated by the GTD-produced far fields of the horn.

Russo *et al.* [4] soon developed edge diffraction theory (EDT) as an approximation applied in solving for backscattering of horns. The diffraction coefficients of GTD were shown to be inadequate for treatment of the horn antenna, and the theory was modified to use diffraction of cylindrical waves at the edges of thin metal sheets. GTD was also modified to solve diffraction from thick edges. EDT gave solutions that were substantially better than those of GTD.

Manuscript received October 1, 1990; revised March 1, 1991.

D. S. Katz, M. J. Piket-May, and A. Taflove are with the Department of Electrical Engineering and Computer Science, Robert R. McCormick School of Engineering and Applied Science, Northwestern University, Evanston, IL 60208.

K. R. Umashankar is with the Department of Electrical Engineering, University of Illinois at Chicago, Chicago, IL 60680.

IEEE Log Number 9101595.

For parabolas, APO has been used to solve for far fields, with various correction factors. Knop and Ostertag [5] showed that APO gave good results compared with experimental data, except in the backscattering region, and that the disagreements were caused by faulty edge-current approximations. They corrected the diffraction coefficients and showed that these corrections had negligible effects in the forward-scattering region, and greatly improved the results in the rear region.

Another method that has been used is the uniform asymptotic theory (UAT). Menendez and Lee [6] used UAT to model simple, two-dimensional radiating structures. UAT generally agrees with GTD, and may be viewed as another refinement, which gives better results under some conditions. Sanyal and Bhattacharyya [7] further refined UAT to give slightly better results than had been previously reported.

In general, high-frequency asymptotic methods work well for modeling electromagnetic wave interactions with electrically large, perfectly conducting structures. However, these approaches are difficult to apply when the structures have reentrant features supporting multiray regions, or material compositions and surface treatments. For these types of structures, the use of other more robust methods is suggested.

It has been shown that MM and FDTD are equally valid methods for finding far-field patterns and radar cross section (RCS) due to scatterers [8], but in the case of very large structures, MM is limited by the amount of computer time and memory available and the possible error accumulation of the matrix solution. Even though MM problems of a large size can be solved with the supercomputers available today, the matrix inversion contained in MM can be a fundamental limit on the use of this method.

One aspect of both FDTD and MM that is only now being studied for the first time is that of dynamic range. The examination of the radiation patterns of the antennas in this paper form a study of dynamic range for objects with a broad angular region of low response. Studies have been done that show that FDTD and MM can both pick up sharp nulls in radiation patterns that are caused by cancellation of field values, but the antennas studied herein are completely different. The low-response region of these antennas is both very broad and is also very gradual. In a region such as this, where the far fields are 50 dB down from peak values, power levels are a factor of 10^{-5} down. This implies accuracy in

0018-926X/91$01.00 ©1991 IEEE

the electric and magnetic fields must be approximately 0.3%, to effectively model these low fields emanating in this direction.

Modeling this huge dynamic range is currently becoming important in many areas: specifically, in two. The first is the design of antennas where sidelobe suppression can be important, and the second is for the design of aerospace vehicles intended to scatter an extremely low fraction of the power of the incident field over a broad angular range. In some cases, especially in the second area, the problems to be solved cannot be studied in the open literature, so it is important to have canonical problems that permit us to examine the important aspects of physics and computational methodology. The horn antenna systems are good canonical problems, because they naturally have this desired broad range of low response in the backward direction.

The results shown here also have applications to other systems of partial differential equations where the desired solutions are required to be accurate to similar levels: namely, one part in three hundred. One example of a system of this type may be found in computational fluid dynamics. In solving the problem of turbulence in air flow near a wing, it may be necessary to have accuracies of one part in one thousand relative to a unit average flow around the wing. A difference of one one-thousandth may make the difference between the flow separating or not. To solve any system with this level of accuracy is a challenge to most numerical methods.

II. FDTD Formulation

A. Standard FDTD (Stepped-Edge)

Finite-differencing was introduced by Yee in the mid-1960's as an efficient way of solving Maxwell's time-dependent curl equations [9]. His method involved sampling a continuous electromagnetic field in a finite region at equidistant points in a spatial lattice, and also at equidistant time intervals. Spatial and time intervals have been chosen to avoid aliasing and to provide stability for the time-marching system [10]. The propagation of waves from a source, assumed to be turned on at time $t = 0$, is computed at each of the spatial lattice points by using the finite difference equations to march forward in time. This process continues until a desired final state has been reached (usually the steady state). This method has been demonstrated to be accurate for solving for hundreds of thousands of field unknowns in a relatively efficient manner on a vector-processing computer [11].

The FDTD method has advantages over other methods in that the required computer memory and required running time are proportional to the number of field components in the finite volume of space being analyzed. In other words, the FDTD method is $\mathbf{O(n)}$, where $\mathbf{n}$ is the number of field components in the region of space being modeled. The method of moments, which involves a matrix inversion step, is $\mathbf{O(n^2)}$ in storage and $\mathbf{O(n^3)}$ in running time, where $\mathbf{n}$ is the size of the matrix.

Initial problems that were overcome in the early 1980's included the termination of the spatial grid while retaining the approximation of the larger size of real space without the addition of reflections from the grid edges [12], [13], the simulation of an arbitrary incident wave [14], and the calculation of the far fields given near-field data over a number of time steps [14]–[16]. The FDTD method is also very straightforward and very robust. However, some problems have existed which have slowed the general acceptance and usage of this method.

One problem, which was simply overcome by the march of technology, was computer resources. Today's computers make it possible to solve for scattering by objects which would have been too large just a few years ago. A second problem is that of visualization, but this is gradually being solved by ongoing work of the authors. Other groups are also making progress in this area. A third problem with the FDTD method for solving practical engineering problems is that of automated geometry generation, but this as well should soon be solved.

The fourth problem, which has recently been solved, is the question of objects that do not fit directly into the standard grid, and that of objects which are smaller than one grid cell. The current FDTD code uses a regularly spaced Cartesian grid with deformed contours along the surface of the modeled object [17]. This is called the contour FDTD method, as opposed to the older, stepped-edge method.

B. Contour FDTD Method

This method involves applying Ampere's and Faraday's laws in those cells where Yee's algorithm is insufficient to describe the geometry of the modeled object, i.e., cells where the intersection of the object's edge and the cell is not along one of the edges or diagonally through the center of the cell. Fig. 1 shows examples of the application of this method. The contour method has been shown to be equivalent to the Yee algorithm in free space [11], and for completeness, this equivalence is demonstrated here for one field component as shown in Fig. 1(a).

By applying Ampere's law along contour C_1 and assuming that the average value of a field component along one side of a contour is equal to the value of that component at the midpoint of that side, one may obtain:

$$\frac{\partial}{\partial t}\int_{\mathbf{S}_1}\mathbf{D}\cdot\mathbf{dS}_1 = \oint_{C_1}\mathbf{H}\cdot\mathbf{d}l_1 \tag{1}$$

$$\begin{aligned}\frac{\partial}{\partial t}\int_{S_1}\epsilon_0 E_z(i,j,k)\mathbf{d}S_1 = {} & H_x\left(i, j-\frac{1}{2}, k\right)\Delta x \\ & + H_y\left(i+\frac{1}{2}, j, k\right)\Delta y \\ & - H_x\left(i, j+\frac{1}{2}, k\right)\Delta x \\ & - H_y\left(i-\frac{1}{2}, j, k\right)\Delta y. \end{aligned}\tag{2}$$

Using the assumptions that $E_z(i, j, k)$ equals the average value of E_z over the surface S_1, $\Delta x = \Delta y = \delta$, and time derivatives may be evaluated through a central difference

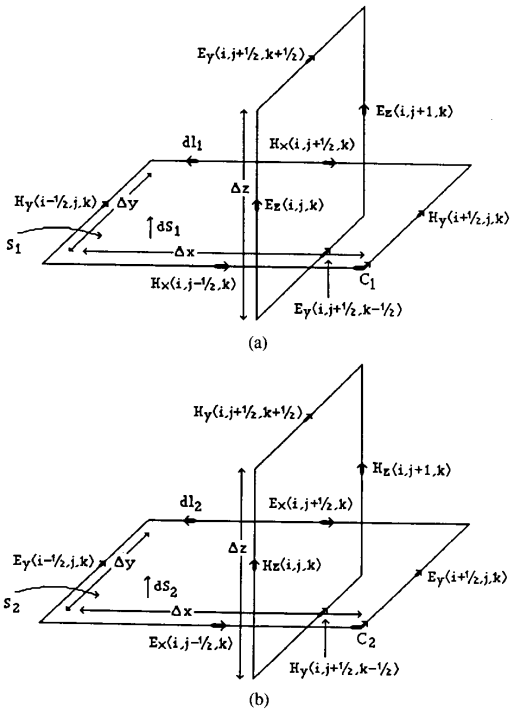

Fig. 1. Examples of spatially orthogonal contours in free space. (a) Ampere's law for E_z. (b) Faraday's law for H_z.

expression, (2) reduces to:

$$\epsilon_0 \delta^2 \left[\frac{E_z^{n+1}(i,j,k) - E_z^n(i,j,k)}{dt} \right] = \left[\begin{array}{l} H_x^{n+1/2}\left(i, j-\frac{1}{2}, k\right) - H_x^{n+1/2}\left(i, j+\frac{1}{2}, k\right) \\ \quad + H_y^{n+1/2}\left(i+\frac{1}{2}, j, k\right) - H_y^{n+1/2}\left(i-\frac{1}{2}, j, k\right) \end{array} \right] \delta \quad (3)$$

where the superscripts indicate the time step for each field value. Solving for $E_z^{n+1}(i, j, k)$ leads to the equation in the Yee algorithm, which may also be derived from the $\nabla \times \mathbf{H}$ equation.

An example of how this may be applied in a two-dimensional transverse electric (TE) case is shown in Fig. 2. Contour C_1 is a normal contour, but Contours C_2 and C_3 are deformed along the dotted lines. The algorithms for the three H_z points within the contours follow, where H_z implies the value inside the contour, E_{y-l} and E_{y-r} indicate the values of the E_y components on the left and right sides of the H_z point, E_{x-t} and E_{x-b} indicate values of E_x components on the top and bottom of the H_z point, and D_a and D_b are constants dependant on the media of the contour:

$$H_z^{n+1} = D_a \cdot H_z^n + D_b \cdot \left(E_{x-t}^{n+\frac{1}{2}} - E_{x-b}^{n+\frac{1}{2}} + E_{y-l}^{n+\frac{1}{2}} - E_{y-r}^{n+\frac{1}{2}} \right) \quad (4)$$

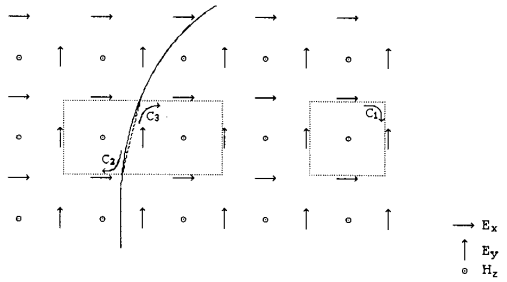

Fig. 2. Example of contour FDTD method, TE case.

$$H_z^{n+1} = D_a \cdot H_z^n + \frac{D_b}{\text{area}\,(C_2)} \cdot \left(l_t \cdot E_{x-t}^{n+\frac{1}{2}} - l_b \cdot E_{x-b}^{n+\frac{1}{2}} + l_l \cdot E_{y-l}^{n+\frac{1}{2}} \right) \quad (5)$$

$$H_z^{n+1} = D_a \cdot H_z^n + \frac{d_b}{\text{area}\,(C_3)} \cdot \left(l_t \cdot E_{x-t}^{n+\frac{1}{2}} - l_b \cdot E_{x-b}^{n+\frac{1}{2}} - l_r \cdot E_{y-r}^{n+\frac{1}{2}} \right), \quad (6)$$

assuming that the curved figure is a perfect electric conductor and that l_l, l_r, l_t, and l_b indicate lengths along the respective (left, right, top, and bottom) sides of the contour, normalized to lengths of exactly 1.0 for the standard contour (C_1.)

As may be seen from (4)–(6), the differences between the last two equations for the deformed contours and the first equation for the standard contour are minimal. Thus, it is a simple matter to transform the stepped-edge model of a scatterer into a true contour model, as long as the number of special cells are small in comparison to the total number of cells in the grid. This is analogous to saying that the number of surface components must be smaller than the number of volume components, which is always true for a reasonably large object.

The rationale behind this approach is that it is more robust and more stable to have a simple algorithm, valid over most of the grid with a slight modification at a few points, than to have a complex algorithm which may be used over the entire grid. The authors believe that this method will lead to reduced computer storage and reduce running times over body-fitted grids and other nonregular grids.

C. Winglike Object (Using Contour FDTD)

As an example of the contour method, a winglike object was modeled. This object was suggested by General Dynamics, Inc. as a test of the accuracy of the contour FDTD method. Fig. 3(a) shows a cross section of the object. The length of the wing is 10 in, and its height is slightly less than 1 in at the center. The object extends 12 in in the third dimension.

To permit direct code-to-code validation of FDTD versus an existing, well-characterized 2-D MM program, it was decided that all numerical modeling runs should be in 2-D (effectively letting the 12-in dimension of the object go to infinity.) This allows an acceptable MM matrix size. In addition, both the FDTD and MM predictions are compared

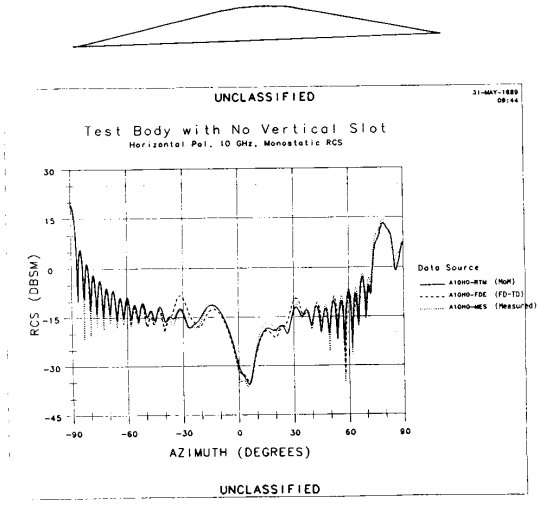

Fig. 3. General Dynamics' test object.

to anechoic chamber measurements (although, of course, this data was obtained for the original 3-D target, not the 2-D idealization).

Fig. 3(b) shows the RCS over a range of angles for the H/H polarization at 10 GHz, and includes the MM data in addition to the FDTD and chamber data. It is clear that the FDTD and MM data virtually overlay each other for observation angles between $+60°$ and $+90°$, where the smooth curve is being directly illuminated and conformal surface modeling is essential to obtain the proper RCS. Excellent agreement is also noted for observation angles between $-90°$ and $-30°$, where the flat side is being directly illuminated. There is some disagreement of the predicted and measured data at grazing illumination. However, the disagreement at these relatively low RCS levels is likely a consequence of the idealized 2-D models versus the 3-D physics actually being modeled in the anechoic chamber.

III. Models and Validations

A. Structures Modeled by FDTD

The work in FDTD modeling of radiating structures begins with a 2-D rectangular waveguide excited by a point source. Next a flare of either 45° or 26.6° is added; these horns are validated against MM for both the aperture fields and the far fields. Next the flared horn is used to excite a parabolically-shaped reflector, and the resulting far-field pattern is examined and compared with a far-field pattern generated from MM. Finally, two 3-D structures are modeled: a rectangular waveguide, and the same waveguide flared into a H-plane sectoral horn. The far-field pattern of the waveguide is compared against an MM model. The far-field pattern of the horn is shown. In addition, a third-dimensional waveguide is used in a hyperthermia application, and a validation is given.

B. Waveguides and Horns in Two Dimensions

The initial object to be modeled is a simple 2-D waveguide. This is one of the simplest radiating objects that can be simulated through the FDTD method, because the rectangular shape leads to a natural stepped-edge model. The waveguide modeled has a width of λ_0, and a length of 5 λ_0. A line source is centered within the guide $\lambda_0/2$ from the closed end. Fig. 4(a) shows a contour map of the fields inside the guide and also emerging from the guide. This picture is clearly the same as any found in an elementary textbook on electromagnetic fields and waves. Fig. 4(b) is a plot of the far-field pattern compared to that obtained using MM. Discrepancies between the two sets of results at levels 35 dB or more below the main lobe are similar to those for the horns discussed in some detail later.

To create the two horn antennas, flares are added to the initial waveguide, adding λ_0 to the total length, with a slope of either 1 or 1/2, corresponding to flare angles of 45° and 26.6° respectively. The 45° horn is not much of a challenge, because of the manner in which a 45° line passes through a square grid. A portion of this model is shown in Fig. 5(a), which demonstrates that by setting the media parameter of the E_z points along the flare to have the properties of metal, the standard FDTD algorithm may be used with no modification.

Fig. 6 shows the agreement between the FDTD results for normalized aperture and phase of the electric field, and results from MM for the 45° horn. It is apparent that these two methods give results which are virtually identical to the human eye.

For the 26.6° horn, which has a flare sloped at 1/2 as seen in Fig. 5(b), only two types of special cells exist (one for the upper flare and one for the lower flare), and the algorithm for these cells may be easily determined by slightly altering the location of the H_x point through which the metal flare passes. The E_z point directly above this becomes a point which is ignored in further computations, but the H_x point above that and the H_y point to its left also become special points. Finally, the H_y point to the right of the E_z point is also ignored in further computations. A similar process will apply to the bottom flare. The algorithm for these special cells is repeated from the end of the waveguide to the end of the horn, along the full length of the flare.

Fig. 7 demonstrates the aperture field agreement of magnitude and phase data between the two methods for the 26.6° horn. As the aperture fields appear the same, the next item of interest was the far-field patterns. This comparison (Fig. 8) showed some agreement in the main lobe, but not anywhere else. This was a matter which caused mild consternation when it was first discovered, because conventional wisdom in this area suggests that near fields which are even slightly different will produce similar far fields, due to the fact that going from near fields to far fields involves an integration, which should average out small errors. Here, however, this is not the case. Extremely close near fields are producing rather distinct far-field patterns.

The first question to be asked is which far-field pattern is correct, if either. The MM model uses 10 sample points per wavelength, and a pulse-current expansion with point matching. Under the assumption that this formulation was suitable for this problem, the number of sample points per wave-

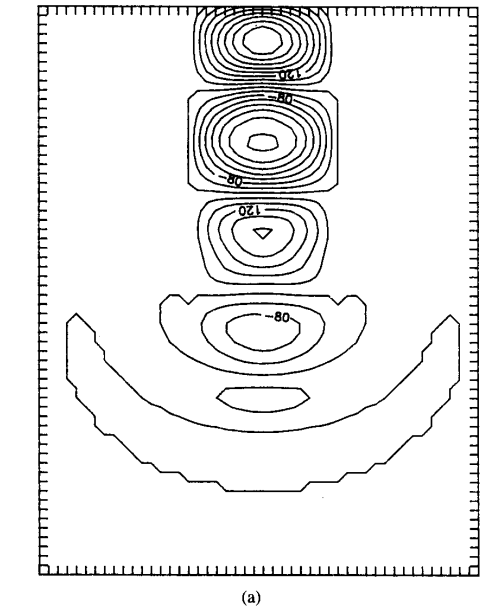

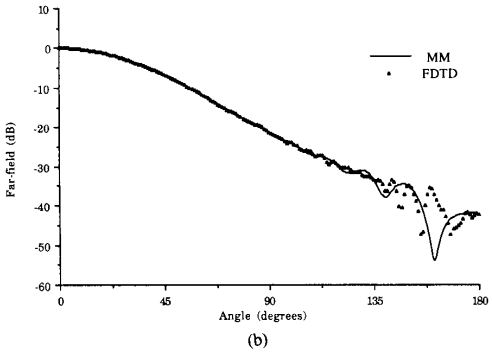

Fig. 4. TM parallel plate wave guide. (a) Near fields. (b) Far fields.

length was varied to 20, 30, and 40. The results of this examination are shown in Fig. 9. It is clear that this variation has little if any effect in the main lobe, but the sampling rate has a definite effect on the sidelobes, and further, the area of the pattern which is affected moves to the sides and down as the number of samples increases. Thus, it has been concluded that the dynamic range of MM is highly dependent on the number of samples per wavelength, and for modeling of objects such as this, 10 samples is not enough, and 40 must be used. In addition, it is possible that other choices of MM current-expansion and weighting functions could give somewhat different results, especially in the low-radiated field region.

For the FDTD model, more possibilities exist to be studied. First, what is the effect of the radiation boundary conditions (RBC's)? For a time-marching code, this is simple to determine by increasing the size the grid in such a manner that the earliest possible reflections from the boundary cannot reach the portion of the grid that is of interest in the number of time steps for which the code is run. This can be consid-

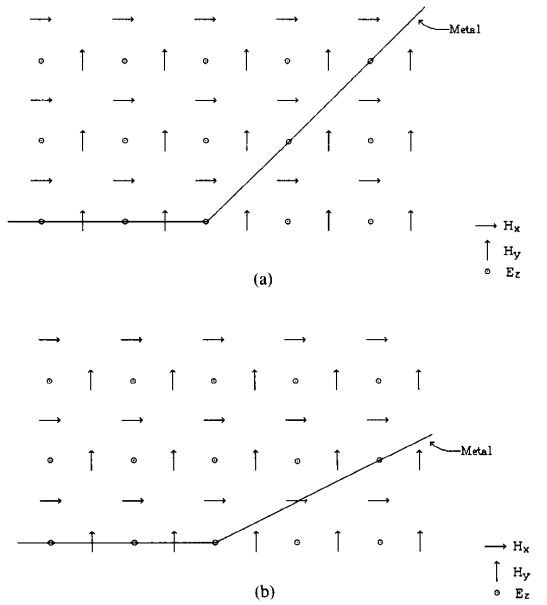

Fig. 5. A portion of the FDTD grid for the TM horns. (a) 45° horn. (b) 26.6° horn.

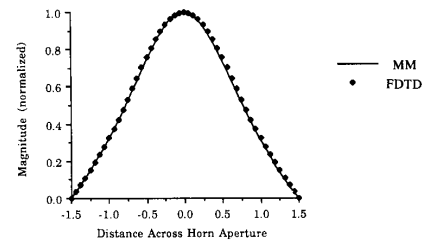

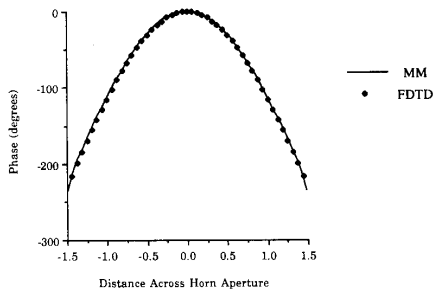

Fig. 6. Normalized aperture data for the 45° horn, TM case. (a) Magnitude. (b) Phase.

ered time-gating out the RBC's. Fig 10(a) shows the results of this time-gating. It is clear that the RBC's perturb the computed pattern, particularly at levels of -40 dB and lower compared to the main beam.

The next change was to move the contour of integration farther from the object while maintaining the time-gating of

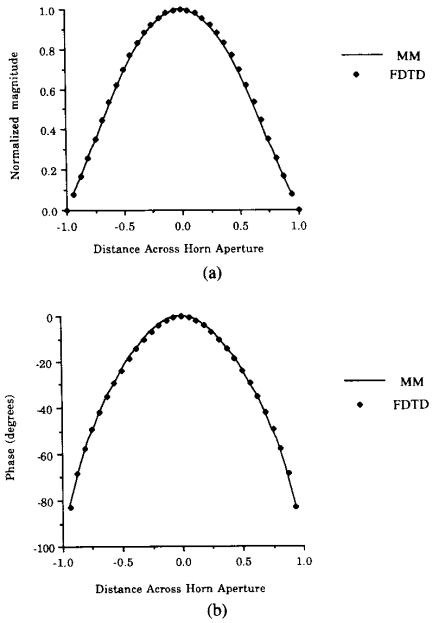

Fig. 7. Normalized aperture data for the 26.6° horn. TM case. (a) Magnitude. (b) Phase.

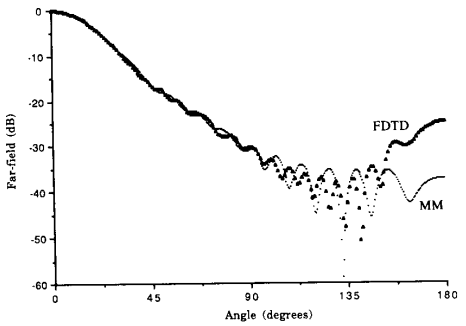

Fig. 8. Initial Comparison for far-field data for the 26.6° horn.

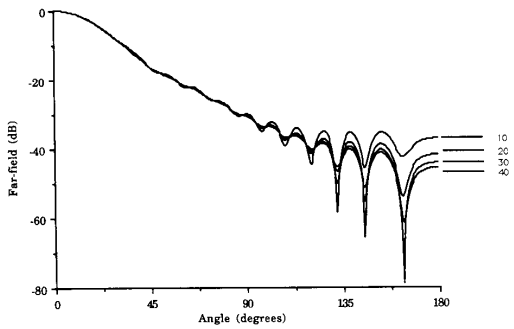

Fig. 9. Far-field data for the 26.6° horn, TM case, MM patterns versus number of samples per λ.

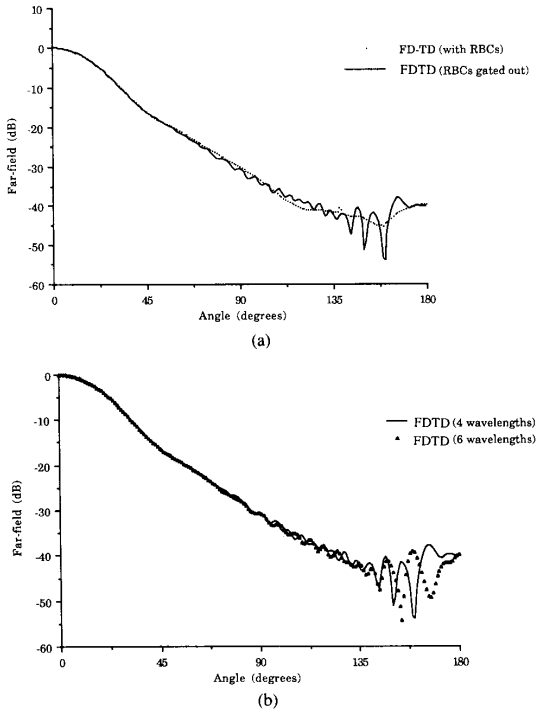

Fig. 10. Far-field data for the 26.6° horn, TM case. (a) FDTD patterns showing effects of RBC's. (b) Patterns showing varied distance from S_a plane to RBC.

the RBC's. In a standard FDTD code which produces good results in most cases, this contour is at least one wavelength away from the object. Fig. 10(b) shows the variation in the far-field pattern, as this distance is increased. It is clear that the placement of the integration contour can also perturb the computed pattern at levels of -40 dB and below.

Fig. 11 compares the most accurate MM and FDTD patterns. There is a substantial improvement over the initial attempt, but there are still differences in the range of the pattern with low-level fields. A change of method of integration of the FDTD near fields was investigated, from trapezoidal rule to Simpson's rule, but this did not make any appreciable difference in the patterns.

Since the possibilities of error in going from the near field to far field have been eliminated by the changes discussed, the next item to examine is the near fields themselves. It has been shown that FDTD requires a grid spacing of 10 cells per wavelength [10], and the models to this point have used a spacing of 16 cells per wavelength. If MM requires a higher spatial sampling rate for this type of model, perhaps FDTD does as well. This is left for future investigation.

C. Horn-Fed Parabolic Antennas in Two Dimensions

After reasonable certainty of the results of the 2-D horns was achieved, the 26.6° horn was placed in two systems containing both a horn and a parabolic reflector. The difference between the systems is the distance between the phase

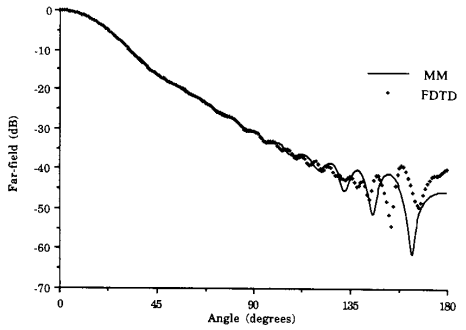

Fig. 11. Far-field data for the 26.6° horn, TM case, FD-TD versus MM, final comparison.

center of the horn and the parabola. This phase center of the horn is located at the focus of the parabola in the first system, and in the second system it is one wavelength closer than the focus. Each system features a parabola with an opening width of 50 λ_0. The two systems, including both the horns and the parabolas, were modeled using the contour method, described above.

The parabola run on a single processor of a Cray 2 used approximately 50 min of CPU time for the FDTD version, and 150 min for the MM version at 40 current sources per wavelength. The latter was shown to be required by a convergence study, as seen in Fig. 12(b).

The far-field plots for these two systems are shown in Fig. 13. The variation in far fields appears most noticeable in the main lobe of the pattern. It appears that placing the horn such that its phase center is slightly closer to the parabola than the focal point (Fig. 13(b)) gives a roughly flat region behind the horn, and only a small amount of scattering behind the parabola.

D. Waveguides and Horns in Three Dimensions

FDTD modeling of two 3-D radiating structures, an open-ended waveguide and a horn antenna, is now considered. The horn is developed from the waveguide, which has the following dimensions. The cross section is $2\lambda_0/3$ in the y direction and $\lambda_0/3$ in the z direction. The length in the x direction is $2\ \lambda_0$. A line source (monopole) oscillates sinusoidally $\lambda_0/3$ from closed end in the x direction, centered in the y direction, and extending from the top to bottom in the z direction. The horn adds a flare perpendicular to the x-y plane, at an angle of 45° to the sides of the waveguide, and extending the full z height of the structure.

Validation of the FDTD model was accomplished by comparison of the computed far-radiated fields with results obtained from a triangular surface patching MM code. The resolution of the MM code was varied from 10 patches per wavelength up to a maximum of 20 patches per wavelength. Little change was noted in comparison with the MM results from lower-resolution models. It is apparent from Fig. 14(b) that MM and FDTD results agree reasonably well for this simple waveguide. Running times for the two codes were also comparable. Fig. 15(b) shows the FDTD computed far-field pattern of the horn.

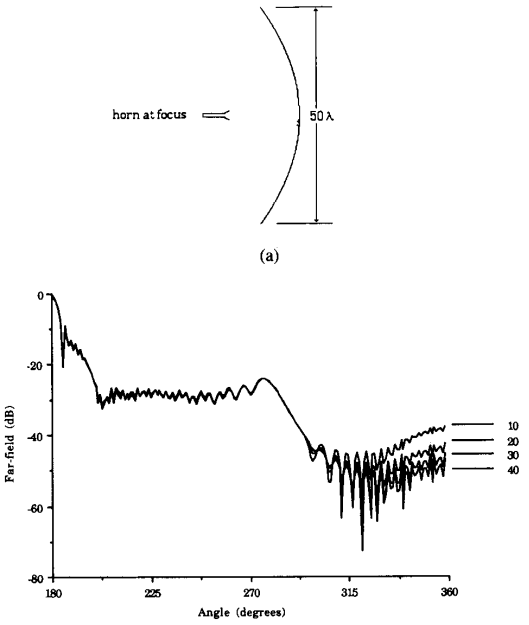

Fig. 12. Far-field data for parabola of 50 λ_0 width, horn fed at focus, MM patterns for various number of patches per wavelength.

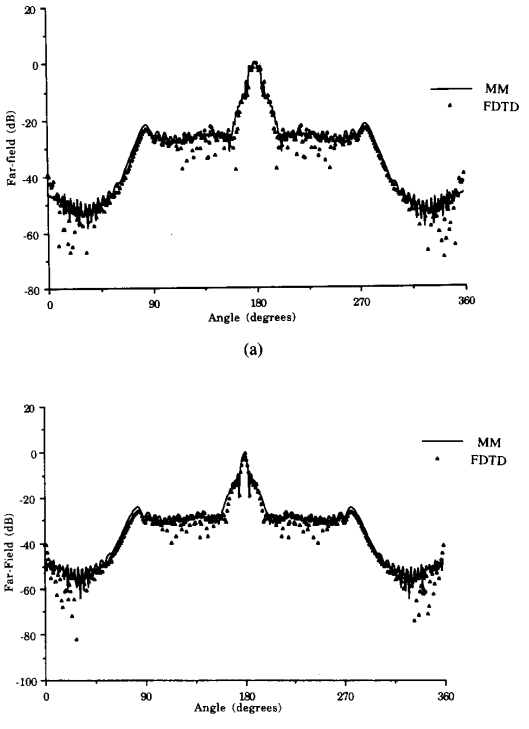

Fig. 13. Far-field data for parabola of 50 λ_0 width. (a) Horn fed at focus. (b) Horn fed λ_0 closer than focus.

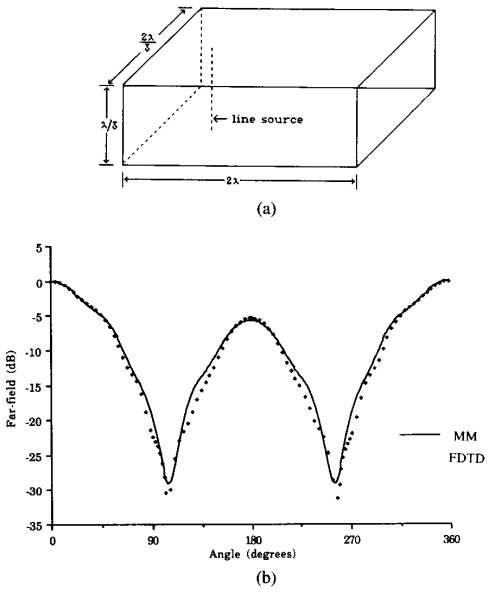

Fig. 14. Three-dimensional waveguide, far fields, ϕ sweep, $\theta = 90°$, E_θ polarization.

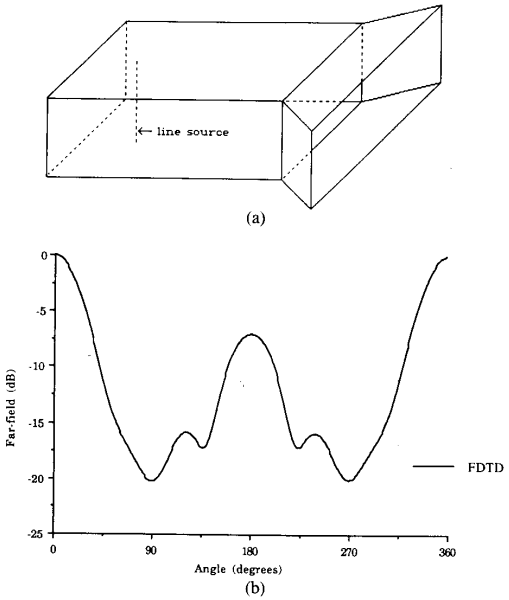

Fig. 15. Three-dimensional flared horn, far fields, ϕ sweep, $\theta = 90°$, E_θ polarization.

E. Hyperthermia Application

Hyperthermia is the use of heat to elevate the temperature of a tumor to greater than 42°C. In combination with radiation or chemotherapy it has shown promising results in the treatment of small surface tumors. Major problems which exist in clinical hyperthermia are: maximizing the therapeutic effects of tumor temperature distribution, minimizing normal tissue damage, and ensuring deposited power is confined to the target tumor volume. Power is applied through electromagnetic (EM) applicators, which can take the form of dielectrically loaded waveguides.

A semi-automated, real-time, patient-specific hyperthermia model has been developed using computer vision system technology and FDTD analysis. [18] Through the use of computer vision, a patient's computed tomography (CT) scans are analyzed to reconstruct a complex, 3-D tissue geometry [19], [20]. These data are transformed into a form suitable for the FDTD method. Luckily, biologic tissue is lossy enough that a stepped-edge geometry is sufficient for good accuracy. The EM applicator is then inserted into the FDTD grid, and the program is run to give an accurate picture of the power deposition. The correct applicator and incident power can then be selected on the basis of this run to provide the desired localization and uniform heat in the tumor volume.

In three dimensions, a water-loaded rectangular waveguide is used to illuminate a tissue structure similar to that modeled by a University of Athens group [21] through an integral equation approach. Fig. 16(a) shows the geometry of the model. In the Athens group's problem, the tissue structure is a layered half-space with 0.5 cm of skin, 1.0 cm of fat, and an infinite layer of muscle. The $5.6 \times 2.8 \times 2.8$ cm^3 waveguide is excited by a line source at 432 MHz, which creates an incident power of 1 W on the tissue structure. The FDTD model assumes the infinite dimensions of the structure may be modeled by half a skin depth in any direction.

Figs. 16(b) and 16(c) show a comparison of the FDTD results and those of the integral equation solver for penetrating electric field contours at the skin–fat interface, and at the fat-muscle interface, respectively. Because of symmetry, only a quadrant of the field distribution is shown.

IV. Summary and Conclusion

This paper has demonstrated that the FDTD method is valid for use in modeling of radiating structures. Based on this validity, the contour FDTD method has been proven to be a new and useful tool for modeling various reflector systems and some biologic problems. While it is recognized that this method has some limitations, the authors can foresee a time in the future when these problems will have been solved, and FDTD will be a standard tool for the analysis of electromagnetic interactions involving large objects.

There are several important issues affecting computational dynamic range. From the discussion of the 26.6° horn, it is clear that neither MM nor current FDTD methods can be blindly applied to antennas or scatterers which have a broad angular range of far fields lower than -40 dB relative to the main lobe or the incident beam. Changing the FDTD gridding to a finer spatial sampling, using brute-force methods to eliminate the effects of the RBC's, and calculating the best integration from the near-field points seem to be ways to achieve more accurate results, and hence, greater dynamic range. However, this reasoning is only valid in two dimensions.

In three dimensions, many things change. The MM matrix size increases by an order of magnitude, which causes the inversion or solution time to increase by three orders of magnitude. For the FDTD code, time-gating out the RBC

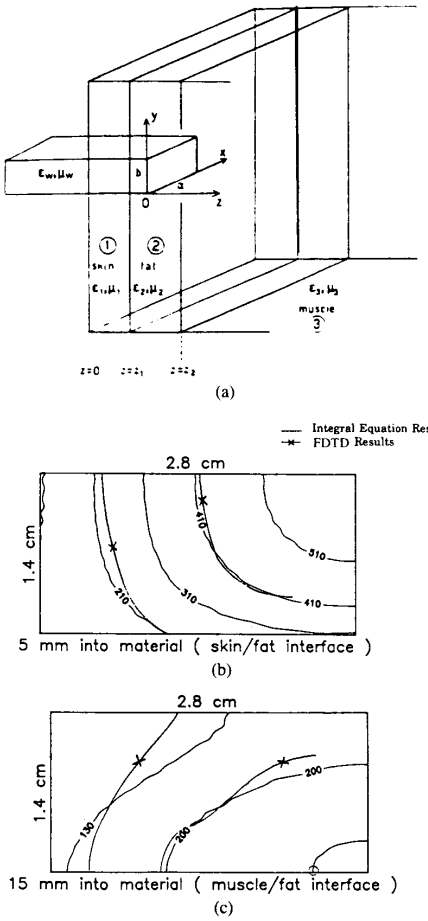

Fig. 16. Hyperthermia application.

reflections is impractical, because it increases the volume of space in which the time marching takes place, which is much worse than simply increasing the area in two dimensions. The fields themselves also change in three dimensions, going from an $r^{-0.5}$ dependance to an r^{-1} dependence. Perhaps this will reduce the negative effects of the RBC's because the fields will be weaker upon reaching the grid boundaries. An important point to note is that for antenna problems, FDTD and MM are similar in that after one large solution is worked out (time marching of fields or matrix inversion,) finding the antenna pattern is simply a matter of a number of integrations or a number of matrix multiplies.

Improved RBC's exist, and these must be examined in both two and three dimensions in the context of problems of this class. In addition, the standard second-order Yee differencing algorithm may itself be unsuitable for problems such as these. It may be necessary to use a fourth-order scheme to achieve the requisite accuracy while maintaining 0.1 λ_0 (relatively coarse) spatial resolution. This also must be examined in both two and three dimensions.

Finally, assuming these modifications are sufficient, large 3-D problems may be attempted. These models will have to be verified experimentally, as the MM equivalent models will be too large to run on today's computers in a reasonable amount of time.

Acknowledgment

The authors wish to thank John Baldauf and S. W. Lee of the University of Illinois at Urbana-Champaign for the validations of the aperture fields for the two-dimensional horns. Thanks also go to Evans Harrigan and Kent Misegades of Cray Research, Inc. for computer resources used for some of the FDTD runs.

References

[1] J. B. Keller, "Diffraction by an aperture," *J. Appl. Phys.*, vol. 28, pp. 426-444, Apr. 1957.

[2] ——, "Geometric theory of diffraction," *J. Opt. Soc. Am.*, vol. 52, pp. 116-130, Feb. 1962.

[3] J. Huang, Y. Rahmat-Samii, and K. Woo, "A GTD study of pyramidal horns for offset reflector antenna applications," *IEEE Trans. Antennas Propagat.*, vol. AP-31, pp. 305-309, Mar. 1983.

[4] P. M. Russo, R. C. Rudduck, and L. Peters, Jr., "A method for computing *E*-plane patterns of horn antennas," *IEEE Trans. Antennas Propagat.*, vol. AP-13, pp. 219-244, Mar. 1965.

[5] C. M. Knop and E. L. Ostertag, "A note on the asymptotic physical optics solution to the scattered fields from a paraboloidal reflector," *IEEE Trans. Antennas Propagat.*, vol. AP-25, pp. 531-534, July 1977.

[6] R. C. Menendez and S. W. Lee, "Analysis of rectangular horn antennas via uniform asymptotic theory," *IEEE Trans. Antennas Propagat.*, vol. AP-30, pp. 241-250, Mar. 1982.

[7] S. Sanyal and A. K. Bhattacharyya, "UAT analysis of *E*-plane near and far-field patterns of electromagnetic horn antennas," *IEEE Trans. Antennas Propagat.*, vol. AP-31, pp. 817-819, Sept. 1983.

[8] A. Taflove, K. R. Umashankar, and T. G. Jurgens, "Comparative time and frequency domain solutions of Maxwells' equations for modeling radar cross section," presented at the Fifth IMACS Symp. Comput. Methods for Partial Differential Equations, Bethlehem, PA, June 19-21, 1984.

[9] K. S. Yee, "Numerical solution of initial boundary value problems involving Maxwell's equations in isotropic media," *IEEE Trans. Antennas Propagat.*, vol. AP-14, pp. 302-307, May 1966.

[10] A. Taflove and M. E. Brodwin, "Numerical solution of steady-state electromagnetic scattering problems using the time-dependent Maxwell's equations," *IEEE Trans. Microwave Theory Tech.*, vol. MTT-23, pp. 623-630, Aug. 1975.

[11] A. Taflove, K. R. Umashankar, B. Beker, F. Harfoush, and K. S. Yee, "Detailed FD-TD analysis of electromagnetic fields penetrating narrow slots and lapped joints in thick conducting screens," *IEEE Trans. Antennas Propagat.*, vol. 36, pp. 247-257, Feb. 1988.

[12] B. Engquist and A. Majda, "Radiation boundary conditions for acoustic and elastic wave calculations," *Commun. Pure Appl. Math.*, vol. 32, pp. 313-357, 1979.

[13] G. Mur, "Absorbing boundary conditions for finite-difference approximation of the time-domain electromagnetic field equations," *IEEE Trans. Electromagn. Compat.*, vol. EMC-23, pp. 1073-1077, Nov. 1981.

[14] K. R. Umashankar and A. Taflove, "A novel method to analyze electromagnetic scattering of complex objects," *IEEE Trans. Electromagn. Compat.*, vol. EMC-24, pp. 397-405, Nov. 1982.

[15] A. Taflove and K. R. Umashankar, "Radar cross section of general three-dimensional scatterers," *IEEE Trans. Electromagn. Compat.*, vol. EMC-25, pp. 433-440, Nov. 1983.

[16] A. Taflove, K. R. Umashankar, and T. G. Jurgens, "Validation of FD-TD modeling of the radar cross section of three-dimensional structures spanning up to 9 wavelengths," *IEEE Trans. Antennas Propagat.*, vol. AP-33, pp. 662-666, June 1985.

[17] T. G. Jurgens, A. Taflove, K. R. Umashankar, and T. G. Moore, "Finite-difference time-domain modeling of curved surfaces," *IEEE Trans. Antennas Propagat.*, to appear.

[18] M. J. Piket, A. Taflove, W. C. Lin, D. S. Katz, V. Sathiaseelan, and B. B. Mittal, "Computational modeling of electromagnetic hyperthermia: Three-dimensional and patient specific," *IEEE Trans. Biomed. Eng.*, to appear.

[19] W. C. Lin, C. C. Liang, and C. T. Chen, "Dynamic elastic interpolation for 3-D object reconstruction from serial cross-sectional images," *IEEE Trans. Medical Imaging*, vol. 7, pp. 225–232, 1989.

[20] W. C. Lin, S. Y. Chen, and C. T. Chen, "A new surface interpolation technique for reconstructing 3-D objects form serial cross sections," *Comput. Vision, Graphics, and Image Processing*, vol. 48, pp. 124–128, 1989.

[21] K. S. Nikita and N. K. Uzunoglu, "Analysis of the power coupling from a waveguide applicator into a three-layered tissue model," *IEEE Trans. Microwave Theory Tech.*, vol. 37, pp. 1794–1801, Nov. 1989.

Daniel S. Katz (S'88) was born in Belleville, IL, on September 11, 1966. He received the B.S.E.E. and M.S. degrees in electrical engineering, both from Northwestern University, Evanston, IL, in 1988 and 1990, respectively.

Currently he is pursuing the Ph.D. degree in the Department of Electrical Engineering at Northwestern University, where he works as a Research Assistant. His research interests include computational modeling of electromagnetic wave propagation, radiation, and scattering.

Mr. Katz is a member of Tau Beta Pi and Eta Kappa Nu.

Melinda J. Piket-May (S'89) was born in Kalamazoo, MI, on July 9, 1965. She received the B.S.E.E. degree from the University of Illinois, Urbana, in 1988, and the M.S. degree in electrical engineering from Northwestern University, Evanston, IL, in 1990.

She is currently pursuing the Ph.D. degree in the Department of Electrical Engineering at Northwestern University, where she works as a Research Assistant. Her research interests include numerical modeling of electromagnetic phenomena with application to VLSI and biomedical problems.

Allen Taflove (M'75–SM'84–F'90), for a photograph and biography please see page 906 of the July 1991 issue of this Transactions.

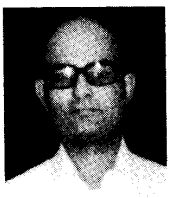

Korada R. Umashankar (S'69–M'75–SM'81) received the B.E. degree from Mysore University, India, in 1962, the M.E. degree from the Indian Institute of Science, Bangalore, India, in 1964, and the Ph.D. degree from the University of Mississippi, University, in 1974, all in electrical engineering.

From 1964 to 1969, he was Assistant Professor and Head of the Department of Electrical Engineering, Karnatak University, Hubli, India. During 1974 and 1975, he was a Postdoctoral Research Associate, and from 1975 to 1977, Assistant Professor of Electrical Engineering at the University of Mississippi, From 1977 to 1979, he was the National Research Council Visiting Fellow at the U.S. Air Force Weapons Laboratory, Kirtland AFB, New Mexico. During 1979 to 1984, he was Senior Engineer at IIT Research Institute, Chicago, IL. During 1984, he joined the faculty of the Department of Electrical Engineering and Computer Science, University of Illinois at Chicago, Chicago, where he is currently a full Professor. His primary research is in the development of analytical and numerical techniques in electromagnetic field theory, EMP/EMC interactions. He has extensively published in open literature research investigations dealing with EM simulation of complex material objects using integral equation methods, finite-difference time-domain techniques, and has been involved in the development of large scale numerical algorithms for super computer applications. He has authored the textbook, *Introduction to Engineering Electromagnetic Fields*, (World Scientific) and has contributed several book chapters in edited research monographs.

Dr. Umashankar is a member of Eta Kappa Nu, Sigma Xi, and URSI Commission B. He is co-chairman of the Technical Committee, the 1992 International APS/URSI, and the NEM Symposium, Chicago, IL.